2007

Circuit for Precision Simulation of a Capacitive Josephson Junction

James A. Blackburn
Wilfrid Laurier University, jabjabjab@cogeco.ca

Circuit for precision simulation of a capacitive Josephson junction

James A. Blackburn
Department of Physics and Computer Science, Wilfrid Laurier University, Waterloo, Ontario N2L 3C5, Canada

(Received 7 February 2007; accepted 5 March 2007; published online 11 May 2007)

A circuit is described which functions as a precision electronic analog of a resistively shunted, capacitive Josephson junction. This design offers significant improvements over earlier simulators, particularly because no analog switches are required, and also because high performance op-amps have been matched to the demands of the circuit. The junction analog is used to generate *I-V* curves, and to model the dynamics when an abrupt bias pulse is applied. The simulator is shown to be very accurate when tested against numerical solutions for the same systems. © *2007 American Institute of Physics*. [DOI: 10.1063/1.2727434]

I. INTRODUCTION

The history of the Josephson junction now stretches back through four decades. Of all the practical applications of Josephson junctions, probably the superconducting quantum interference device magnetometer has had the most widespread and significant impact. Early on, there was considerable interest in the possibility of building a superconducting computer based on the ultrafast switching properties of Josephson devices. Nowadays there is a renewed focus on superconducting computing with proposals to implement qubits in the form of Josephson circuits.[1] Another topic of current interest centers on the switching of a junction out of the zero voltage state via resonant activation from the shallow effective potential well associated with a fixed bias current just below the critical value.[2]

The development of superconducting circuits has traditionally relied heavily on computer simulations that generate numerical solutions of the differential equations which govern each specific system. The earliest nondigital approach utilized a commercial analog computer,[3] a total of 48 operational amplifiers were required in the patching scheme.

From the outset there were proposals to model Josephson junctions with analog circuits specifically designed to mimic the junction dynamics. That is to say, the time dependent voltages appearing in the circuits obeyed differential equations which were isomorphic to those describing the superconducting circuit containing one or more Josephson devices. Such an approach constitutes a fundamental alternative to the digital computer modeling route. Electronic analogs of this type are, in reality, nondigital computers designed to simulate a particular physical system.

Over the years, there have been a number of such analog simulations, beginning with Hamilton's 1972 design which used type 741 op-amps and MC1494 multipliers as the building blocks.[4–16] One class of simulator was based on the association of the phase across a Josephson junction with the difference between the outputs of two oscillators, one a reference oscillator and the other a voltage-controlled oscillator (VCO). In some of these designs,[10,11,16] the voltage-controlled oscillator function was performed by a type 555 integrated circuit, whereas Henry *et al.*[12] employed the AD537 voltage-to-frequency converter. Low pass filters were employed to extract the analog of the Josephson sine term.

A different class of simulator, typified by Refs. 7 and 9, has no reference oscillator, but is based instead on a classic voltage integrator followed by a precision triangle-to-sine conversion subcircuit. A design for the feedback VCO[14] was employed in an earlier investigation of Josephson junctions in superconducting loops.[15] That circuit was used subsequently to study the characteristics of a junction coupled to a transmission line[17] and of a pair of junctions coupled by a transmission line.[18] Similar to the design of Magerlein, it required analog switches (an MC14053 multiplexer was used) to flip the polarity of the integrator input whenever a maximum or minimum was reached.

In this paper, a significantly improved design for a Josephson junction analog is described. It entirely avoids the need for integrated circuit switches with their attendant noise and speed problems and, furthermore, it utilizes high performance op-amps to additionally minimize noise and improve bandwidth. There are relatively few components and no critical adjustments are required. This circuit thus goes beyond the usual role of simulators as demonstration apparatus and becomes, because of its stability and accuracy, a tool for quantitative research investigations of such time dependent phenomena as noise driven and resonant activation from the potential wells associated with biased Josephson junctions.[19,20] Early on, Werthamer[3] aptly noted the particular benefit of the analog approach: System parameters can be continuously varied by "turning a knob" and the results appear immediately. Thus as a package, an analog simulator together with an oscilloscope with data saving capabilities and an arbitrary function generator becomes a powerful interactive *experimental* system.

II. CIRCUIT DESIGN

The simulation circuit is depicted in Fig. 1. Component values were: $R=3.98$ K, $C=1$ μF, $R_C=12.5$ K, and $R_b=4.07$ K. Summing the currents at the inverting input of the op-amp gives

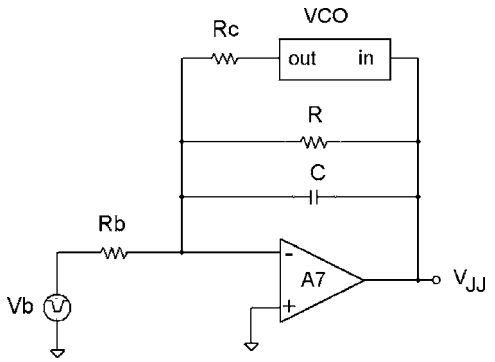

FIG. 1. Schematic of a Josephson junction electronic analog based on an op-amp and a voltage controlled oscillator (VCO).

$$\frac{\mathrm{VCO_{out}}}{R_C}+\frac{V_{JJ}}{R}+\frac{dQ_C}{dt}=-\frac{V_b}{R_b}, \tag{1}$$

where the op-amp output voltage is denoted as V_{JJ}, and V_b is an applied bias. But $Q_C=CV_{JJ}$ and therefore

$$\frac{\mathrm{VCO_{out}}}{R_C}+\frac{V_{JJ}}{R}+C\frac{dV_{JJ}}{dt}=-\frac{V_b}{R_b}. \tag{2}$$

The VCO subcircuit, discussed in detail below, implements the input-output relationship

$$\mathrm{VCO_{out}}=\alpha\sin\left[2\pi k\int \mathrm{VCO_{in}}dt\right]. \tag{3}$$

Here, $\mathrm{VCO_{in}}=V_{JJ}$. Defining a phase variable

$$\theta=2\pi k\int V_{JJ}dt. \tag{4}$$

Equation (2) can be expressed as

$$\ddot{\theta}+\frac{1}{R}\sqrt{\frac{R_C}{2\pi k\alpha C}}\dot{\theta}+\sin\theta=-\frac{V_bR_C}{\alpha R_b}, \tag{5}$$

where overdots indicate derivatives with respect to normalized time $t^*=t/\tau$, with

$$\tau=\sqrt{CR_C/2\pi k\alpha}. \tag{6}$$

An analogous equation governs the superconducting phase across a current biased finite capacitance Josephson junction

$$\ddot{\phi}+\frac{1}{Q}\dot{\phi}+\sin\phi=\frac{I_b}{I_C}, \tag{7}$$

where time has been scaled to the reciprocal of the Josephson plasma frequency $\omega_P=\sqrt{2eI_C/\hbar C}$ and $Q=R_J\sqrt{2eI_CC/\hbar}$ with junction resistance R_J, capacitance C, critical current I_C, and bias I_b. Comparing Eqs. (5) and (7), it is apparent that

$$Q=R\sqrt{\frac{2\pi k\alpha C}{R_C}}. \tag{8}$$

Note that the equivalent of a positive bias on a junction [right-hand side of Eq. (7)] is produced in the analog circuit by a negative applied voltage V_b [right-hand side of Eq. (5)]. Also observe that Q can be set with resistor R without changing either the time scaling or the relative bias.

A. VCO design

The heart of the simulator is the voltage controlled oscillator, shown in Fig. 2. The central element of the VCO is amplifier $A3$ which is a standard analog integrator. Operational amplifiers $A1$ and $A2$ are configured as noninverting Schmitt triggers[21] which are characterized by hysteresis: The op-amp output will stay high until the input drops below a threshold V_{TL}, at which point the output rapidly switches to its maximum negative value. Once this switching has taken place, the output can only return to its maximum positive value when the input rises above an upper threshold V_{TH}. The difference $(V_{TH}-V_{TL})$ is the hysteresis. The resistors in the $A1$ configuration set $V_{TH}=-V_{TL}=0.003V_H$ where $V_H\approx 10$ V is determined by the back-to-back 1N960 (9.1 V) Zener diode limiter.[21] The switching thresholds are thus about ±30 mV. Note that the limiter output of close to ±10 V means that $M1$, an AD632 multiplier with an internal divide-by-ten, effectively counteracts the effect of negative polarity VCO inputs.

The resistors in the $A2$ configuration set $V_{TH}=-V_{TL}=0.122V_H$ where $V_H\approx 7.5$ V is determined by the back-to-back 1N754 (6.8 V) Zener diode limiter. The switching thresholds here are thus about ±0.92 V. In essence, the integrator will alternate between positive going segments and negative going segments, switching from one to the other each time its amplitude reaches the threshold for Schmitt $A2$ (±0.92 V).

Suppose a design objective is to produce a VCO with a response of 1000 Hz/V. For one volt dc at the VCO input, the integrator will receive 0.1×7.5 from $M2$, where the first factor accounts for the internal ÷10 of the AD632 multiplier. The integrator output will be a linear ramp which must take 0.5 ms to cover the voltage interval between the trip levels set by Schmitt $A2$, namely 2×0.92; so the slope of the ramp must be 3680 V/s. This can be achieved if $0.75\times(RC)^{-1}$ equals 3680, and so, for example, one could choose $C=0.01$ μF and $R=20$ K as shown in the schematic. Hence for any dc voltage at the VCO input, a triangle wave will be generated with amplitude ±0.92 V and a conversion factor of 1000 Hz/V.

Figure 2(b) gives the schematic of the triangle-to-sine converter. Op-amp $A4$ is a simple buffer; $A5$ is an inverting amplifier which permits adjustments to the triangle wave amplitude being passed to the six diode wave shaper. A final amplifying stage, $A6$, sets the VCO sinewave output amplitude.

III. PERFORMANCE

In Ref. 7 the alternating reversals of integrator output required to generate the desired triangle wave were accomplished with an integrated circuit analog switch (DG303), while in Refs 14, 15, 17, and 18 the VCO employed an MC14053 for a similar purpose. As can be seen in Fig. 2, the design presented here has no analog switches—the Schmitt triggers provide the equivalent functions while avoiding the necessity for digital addressing of switches as well as possible noise artifacts. A second important feature of this design is the choice of type OP27 operational amplifiers, which

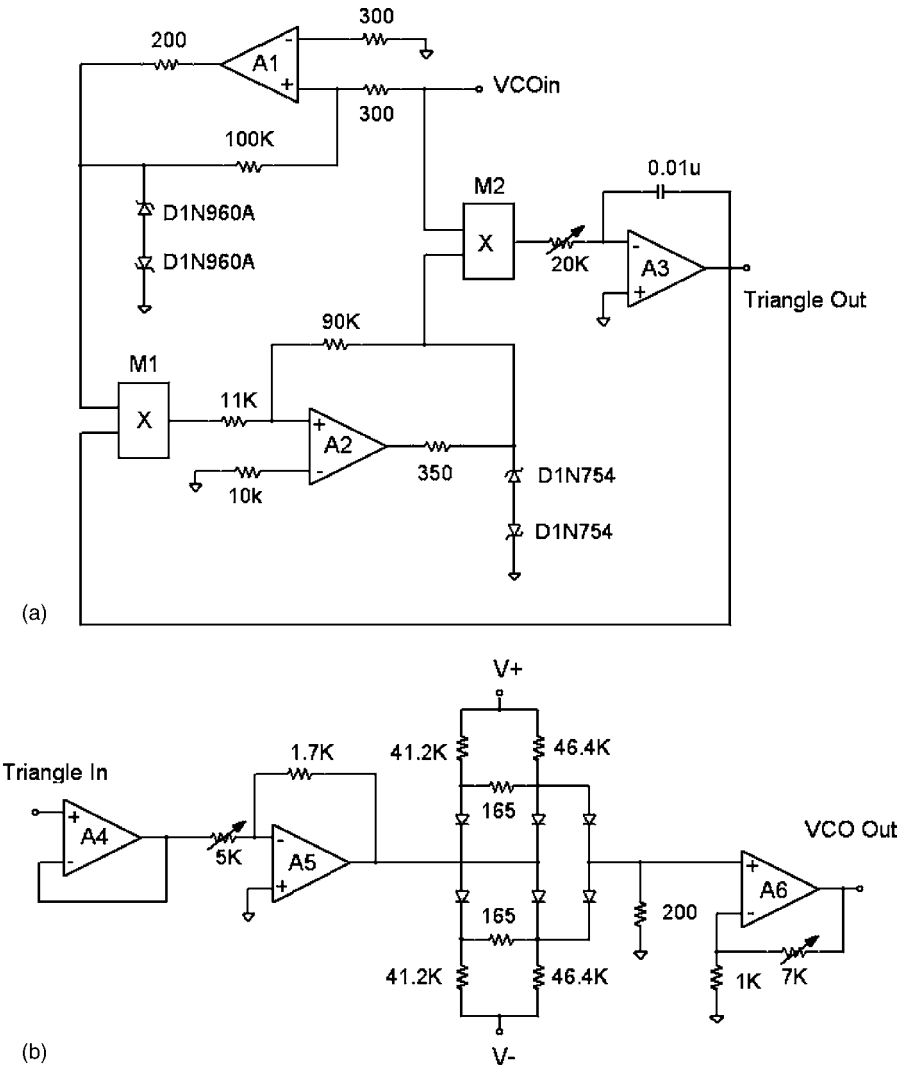

FIG. 2. Schematic of the voltage controlled oscillator (VCO). (a) Main portion that generates a triangle wave whose frequency depends on the input voltage. (b) Triangle-to-sine converter. The op-amps are Analog Devices type OP27; M1 and M2 are four quadrant multipliers type AD632. The diodes in the sine converter are 1N914.

are rated as low noise, high speed devices. All of the circuits already cited employed either type 741 or, in the case of Refs. 7 and 9, type TL081, 082, 083 op amps. The OP27 is a sort of "super" 741 offering a much higher performance in a package that is, with the exception of external offset connections, pin compatible with the 741. As a comparison, the OP27 has a maximum input offset voltage of 25 μV, about one hundred times smaller than either the TL08x series or the 741. Similarly, the maximum input bias current for the OP27 is specified as ±40 nA, about one-tenth of the figure for the 741. The slew rate for the OP27 is given as 2.8 V/μs, five times that of a 741. The AD632 four quadrant multiplier is also a premium component, classified as a low error, low noise chip.

Real time output data $V_{JJ}(t)$ were recorded on a Tektronix TDS 2022 digital storage oscilloscope. Bias signals $V_b(t)$ were produced by a Tektronix AFG 3101 arbitrary function generator. When simple dc voltages were required, a Xantrex XDL35–5TP digital power supply was used.

It was possible to isolate the VCO subcircuit for the purpose of calibration. Three trimpots are indicated on the schematic: One is used to set the conversion factor k, another optimizes the input magnitude to the diode sine converter, and the final trimpot adjusts the sinewave output amplitude α.

A number of dc input voltages were applied and the resulting VCO frequency was read from the oscilloscope. These data are plotted in Fig. 3. The slope of the linear fit yields a conversion factor for the VCO of $k=987.6$ Hz/V.

The action of the triangle-to-sine converter subcircuit is illustrated by Fig. 4. It is imperative that the VCO produce as high fidelity a sine wave as possible since the sine term plays a key role in the governing Eq. (5). The purity of the sine output depends sensitively on the amplitude of the incoming

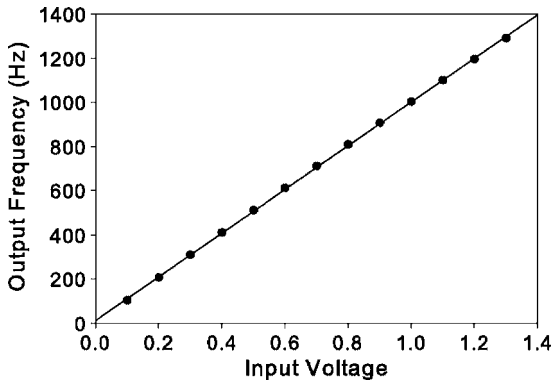

FIG. 3. Calibration of the VCO. From the slope, the conversion factor k is found to be 987.6 Hz/V.

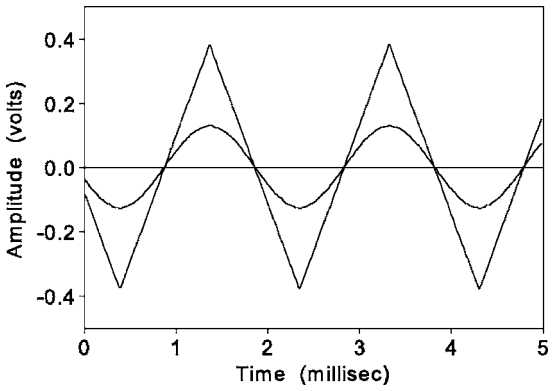

FIG. 4. Oscilloscope data showing the action of the six diode sine converter.

triangle wave. It was found that an effective way to optimize the sine wave was to adjust the triangle amplitude via the trimpot on the input of $A5$ while observing a real time Fast Fourier Transform (FFT) display of the diode array output on the digital oscilloscope. The "best" setting minimizes all harmonics except the fundamental, thus reducing distortion. A sample FFT spectrum, plotted from oscilloscope data, is shown in Fig. 5. Clearly all harmonics are exceedingly small.

The classical signature of a Josephson junction is its bias current versus time-averaged voltage characteristic. For an underdamped junction (finite capacitance) the I-V characteristic is hysteretic. To observe the counterpart of this on the electronic simulator, a (negative) bias voltage V_b must be applied and the time-average of the output V_{JJ} evaluated. This averaging was performed directly by the digital oscilloscope. Because of the anticipated hysteresis, V_b must first be taken up in steps, then reduced downward in steps. The experimental results are shown in Fig. 6. The critical bias voltage can be predicted from Eq. (5); it is

$$V_{bc} = -\frac{\alpha R_b}{R_C}, \tag{9}$$

which, using the nominal resistance values stated earlier, gives −0.326 V. The experimentally observed value is very close to this: −0.331 V. The transition to the running state was very sharp, and the uncertainty in the value of V_{bc} was

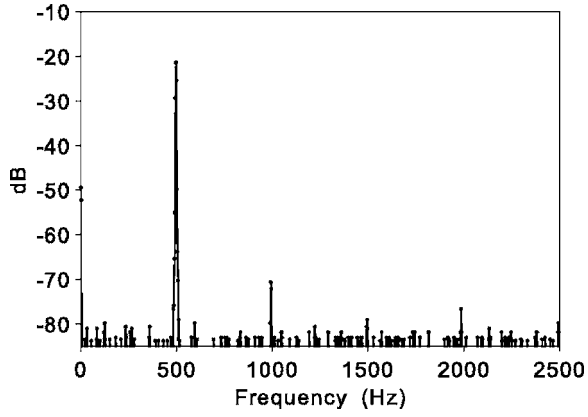

FIG. 5. FFT spectrum (taken from the TDS 2022 oscilloscope) showing of the spectral content of the output from the six diode sine converter when the input triangle wave amplitude is optimized. The fundamental in this case is at 500 Hz.

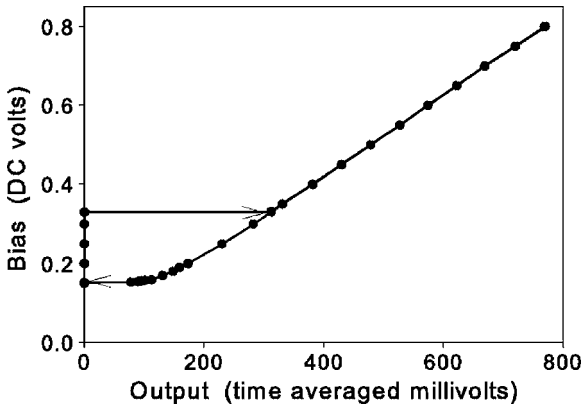

FIG. 6. Hysteretic characteristic from the electronic analog (oscilloscope data). The vertical scale indicates only the magnitude of the applied bias voltage. This response is equivalent to the dc I-V characteristic of a Josephson junction.

only ±1 mV. The measured bias at the lower switchback was 0.153 V, also ±1 mV, giving a precise value for the hysteresis parameter of $(0.153)/(0.331)=0.462$.

With the nominal component values stated, one would anticipate from Eq. (8) that $Q=2.80$. Numerical solutions of Eq. (7) obtained with a fourth-order Runge-Kutta algorithm were used to search for a value for Q that resulted in a hysteresis parameter which matched the simulator result of 0.462. The best choice is shown in Fig. 7. This closest agreement happened for $Q=2.66$, consistent with the anticipated value. It is worth noting that although the various resistance and capacitance values are not usually known with a high precision, the hysteresis parameter *is* determined quite accurately from the experiment, and thus a very good value of Q can be inferred from the data.

Time averaging, as when simulating I-V characteristics, has the potential for masking subtle but sometimes important temporal details. More stringent tests involve transient phenomena, as will now be illustrated. To begin, it is useful to invoke the well-known fact that an equation such as Eq. (5) can be interpreted as describing the dissipative motion of a "particle" on a tilted washboard potential of the form

$$U(\theta) = -\left[\left(\frac{V_b}{V_{bc}}\right)\theta + \cos\,\theta\right]. \tag{10}$$

Without an external bias, the potential is just an inverted cosine as indicated in Fig. 8, and the particle would reside in

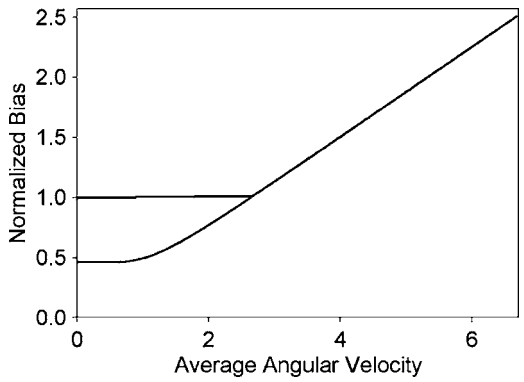

FIG. 7. Hysteresis curve from the numerical solution of Eq. (7) with $Q=2.66$.

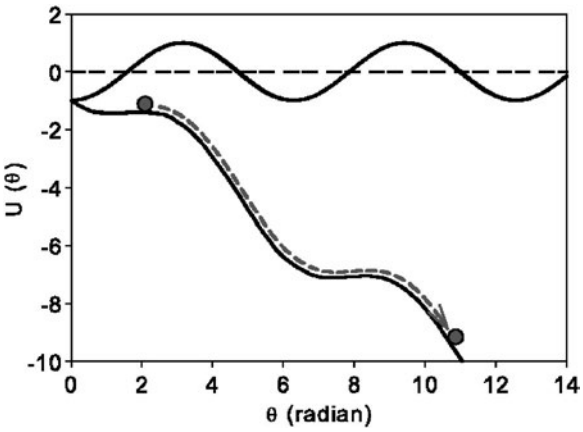

FIG. 8. Washboard potential according to Eq. (10) with no applied bias (upper curve) and an applied bias which is 90% of critical (lower curve).

the minimum at $\theta=0$. If the bias is increased slowly, the washboard tilts, with the wells becoming progressively shallower, as depicted in the figure. When a critical bias is reached, the well becomes flat and the particle can slip out, bumping down the washboard. However, if the bias is increased more abruptly, then it is possible for an impulsive reaction to cause the particle to escape from the well prematurely—that is, when the bias is still somewhat less than the critical value. The details of this sort of early escape will clearly depend sensitively on the rate at which the tilting is imposed.

As an example of this phenomenon, a bias *pulse* was applied to the analog simulator, as depicted in Fig. 9. The pulse amplitude was chosen to be 0.300 V, less than the critical value of 0.331 V, but because the onset is rather sudden (1 ms rise and fall times), the junction just manages to switch to a running state. Looking at the figure, this can be visualized as an initial impulsive kick delivered on the leading edge of the bias pulse, followed by a slowing of the particle as it rises toward the lip of the potential well. If the kick is sufficient, as in this illustration, the particle has enough momentum to carry it over the lip (at around 10 ms), after which it bounces down the washboard. When the bias pulse is switched off, the oscillations cease and a damped plasma oscillation is seen. Turning off the bias is analogous

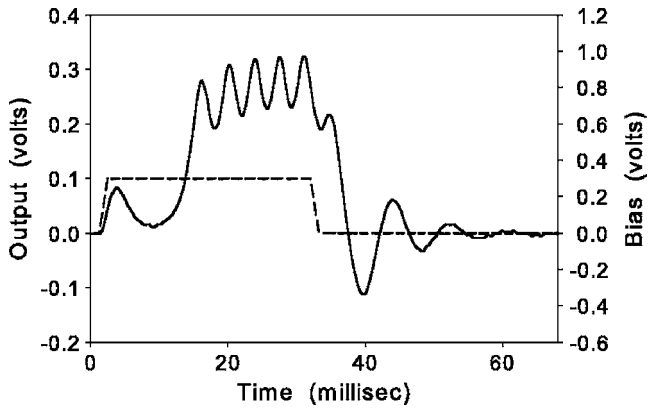

FIG. 9. Simulator output (oscilloscope data) when a bias pulse (dashed) is applied. This pulse does not quite reach the critical value of 0.331 V, but oscillations are nevertheless triggered.

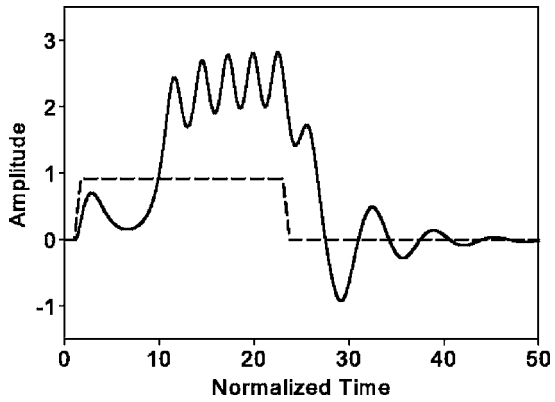

FIG. 10. Numerical simulation results for $Q=2.66$ showing the response of a junction to a bias pulse (dashed) with equivalent parameters to compare with the experimental data shown in Fig. 9.

to restoring the potential to an untilted condition, as in the upper part of Fig. 8.

This experiment can be compared to numerical simulations by solving Eq. (7) with $Q=2.66$ and a correspondingly chosen bias pulse. The result is shown in Fig. 10. The precise agreement with the electronic analog is quite evident.

The time scales deserve a comment. Because of the normalizing in Eq. (6), the natural frequency, without dissipation, is just $\omega_0=1$. For the electronic circuit, from Eq. (5), the natural frequency would also be one, but that equation has rescaled time, with units $\tau=\sqrt{CR_C/2\pi k\alpha}$, which for the component values used here is $\tau=1.42$ ms. A precise calibration can be obtained by comparing the oscillation periods for equivalent running states in numerical solutions and in the circuit (output from scope data) when each is given the same normalized bias at some level slightly larger than the critical value, such as 1.200. When this was completed, the time calibration was found to be $\tau=1.304$ ms. Therefore, the range of the horizontal axis in Fig. 10 (50 time units) corresponds to 65 ms in the experimental record of Fig. 9. Again, the agreement between numerical and electronic simulations is very close. Because of the normalization in Eqs. (5) and (7), a plasma oscillation would have a period 2π. In simulator time, this period would be $2\pi\times1.304=8.19$ ms. The damped plasma oscillations in Fig. 9 are in good agreement with this number.

To summarize, the simulator is fully characterized by three quantities: τ, Q, and V_{bc}. These may be evaluated from known component values using Eqs. (6), (8), and (9). When component values are not known with sufficient accuracy, the following experimental procedures will yield more precise results. For V_{bc}, simply measure the bias voltage which triggers a running solution. For Q, measure the hysteresis parameter and then seek a match to a numerical solution. For τ, measure the period of a free running state and compare it with numerical solutions. Once calibrated, there is no further need of digital computations, and the simulator then can be used to study system dynamics under various bias input waveforms.

IV. DISCUSSION

The objective in designing this electronic analog of a Josephson junction was to realize unprecedented accuracy

and low intrinsic noise. It is evident from the data reported that the circuit, in combination with a digital oscilloscope and arbitrary function generator, constitutes a precise system for analog computation. The benefit of this electronic approach over conventional numerical simulation is, primarily, real time interactivity. Once accuracy is assured through careful design, the analog system affords a means of rapidly assessing system dynamics with the extra, and significant, benefit of user involvement. The interplay between user input and system response offers an enormous potential advantage in exploring the behavior of such complex physical systems. The precision and stability achieved in this simulator could, for example, facilitate future studies of resonant or noise activation from effective potential wells in Josephson devices.

ACKNOWLEDGMENTS

The author thanks Niels Grønbech-Jensen for suggesting the need for a state of the art electronic Josephson junction simulator. The circuit and custom board were built by Manfred Gartner. Funding was provided by the Natural Sciences and Engineering Research Council of Canada.

[1]P. Bertet, I. Chiorescu, K. Semba, C. J. P. M. Harmans, and J. E. Mooij, Phys. Rev. B **70**, 100501 (2004).
[2]M. H. Devoret, J. M. Martinis, D. Esteve, and J. Clarke, Phys. Rev. Lett. **53**, 1260 (1984).
[3]N. R. Werthamer and S. Shapiro, Phys. Rev. **164**, 523 (1967).
[4]C. A. Hamilton, Rev. Sci. Instrum. **43**, 445 (1972).
[5]C. K. Bak and N. F. Pedersen, Appl. Phys. Lett. **22**, 149 (1973).
[6]K. H. Gundlach, J. Kadlec, and W. Heller, J. Appl. Phys. **48**, 1688 (1977).
[7]J. H. Magerlein, Rev. Sci. Instrum. **49**, 486 (1978).
[8]D. B. Tuckerman, Rev. Sci. Instrum. **49**, 835 (1978).
[9]A. Yagi and I. Kurosawa, Rev. Sci. Instrum. **51**, 14 (1980).
[10]R. W. Henry and D. E. Prober, Rev. Sci. Instrum. **52**, 902 (1981).
[11]D. E. Prober, S. E. G. Slusky, R. W. Henry, and L. D. Jackel, J. Appl. Phys. **52**, 4145 (1981).
[12]R. W. Henry, D. E. Prober, and A. Davidson, Am. J. Phys. **49**, 1035 (1981).
[13]D. G. Jablonski, J. Appl. Phys. **53**, 7458 (1982).
[14]B. Wu, Z. Yang, J. A. Blackburn, H. J. T. Smith, and M. A. H. Nerenberg, Phys. Rev. B **37**, 3349 (1988).
[15]J. A. Blackburn, B. Wu, and H. J. T. Smith, J. Appl. Phys. **64**, 3112 (1988).
[16]C. M. Pegrum, W. S. C. Gurney, and R. M. Nisbet, IEEE Trans. Magn. **25**, 1404 (1989).
[17]J. A. Blackburn, H. J. T. Smith, and N. Grønbech-Jensen, J. Appl. Phys. **70**, 2395 (1991).
[18]H. J. T. Smith, J. A. Blackburn, and N. Grønbech-Jensen, J. Appl. Phys. **74**, 5101 (1993).
[19]N. Grønbech-Jensen, M. G. Castellano, F. Chiarello, M. Cirillo, C. Cosmelli, L. V. Filippenko, R. Russo, and G. Torrioli, Phys. Rev. Lett. **93**, 107002 (2004).
[20]C. Schmitt, B. Dybiec, P. Hänggi, and C. Bechinger, Europhys. Lett. **74**, 937 (2006).
[21]D. A. Neamen, *Microelectronics: Circuit Analysis and Design*, 3rd ed. (McGraw-Hill, New York, 2007), pp. 1085, 1089.